The Rotational Zeeman Effect of Imines

II. Cis- and Trans-Ethanimine and Trans-Syn- and Trans-Anti-Propenimine, their g-Tensors, Magnetic Susceptibility Anisotropies, Molecular Electric Quadrupole Moments, ^{14}N Nuclear Quadrupole Coupling Constants, and ^{14}N Spin-Rotation Coupling Constants; a Microwave Spectroscopic Study Combined with Quantum Chemical Calculations

H. Krause* and D. H. Sutter

Abteilung Chemische Physik im Institut für Physikalische Chemie
der Christian-Albrechts-Universität zu Kiel

Z. Naturforsch. **46 a**, 785–798 (1991); received June 3, 1991

The zero field ^{14}N-hfs-multiplets and the high-field Zeeman-hfs-multiplets of low-J rotational transitions of the title compounds were observed in a flash pyrolysis setup under high-resolution conditions. From the zero-field hfs patterns the ^{14}N spin-rotation coupling constants and the ^{14}N nuclear quadrupole coupling constants were obtained. From the high-field Zeeman-hfs-multiplets, the diagonal elements of the molecular g-tensor and the anisotropies in the diagonal elements of the molecular magnetic susceptibility tensor were determined and were used to derive the diagonal elements of the molecular electric quadrupole moment tensor. INDO calculations and restricted Hartree-Fock self consistent field calculations with a basis of TZVP quality were carried out at the experimental structures and critically compared to the experimental results.

Introduction

The present study is the second in a sequence of rotational Zeeman effect studies of small imine compounds. The analysis of the rotational Zeeman effect gives experimental values for the anisotropies in the diagonal elements of the molecular magnetic susceptibility tensor and of the diagonal elements of the molecular g-tensor, and it gives direct experimental access to the molecular electric quadrupole moment tensor. The analysis of the zero-field ^{14}N hyperfine (hfs) multiplets, which is a prerequisite for the subsequent analysis of the Zeeman-hfs-multiplets, gives information on the vibronic expectation value for the electric field gradient tensor at the ^{14}N nucleus and on its spin-rotation coupling tensor.

The molecular magnetic susceptibilities are of interest in the context of additivity rules from local increments and for the assessment of molecular field induced ring currents in aromatic molecules. The molecular electric quadrupole moments play an important role for the intermolecular forces at close range (→ local substructures in liquids, → shapes of van der Waals complexes, etc.).

Furthermore the molecular electric quadrupole moments and the quadrupole coupling constants, the latter closely related to the electric field gradients at the quadrupole nuclei in the molecules, are of interest for the comparison with quantum chemical calculations. While the molecular quadrupole moments probe the quality of the electronic wavefunctions in the outer regions of the electron cloud, the field gradients probe the wavefunction in the immediate surroundings of the quadrupole nuclei. We therefore found it interesting to run standard semiempirical and ab initio quantum chemical programs on the experimental structures in order to get a feeling for their predictive power.

Thus the present contribution is subdivided into two parts. In the first part we describe the experiments and their analysis and in the second part we present the results of the quantum chemical calculations and compare them with the experimental results.

Experimental and Analysis

The pyrolysis flow system, the spectrometer, and the line shape analyses used to derive accurate satellite

* In partial fulfillment of the requirements for the PhD thesis.

Reprint requests to Prof. Dr. Dieter H. Sutter, Abteilung Chemische Physik im Institut für Physikalische Chemie, Christian-Albrechts-Universität zu Kiel, W-2300 Kiel 1, Federal Republik of Germany.

0932-0784 / 91 / 0900-0785 $ 01.30/0. – Please order a reprint rather than making your own copy.

frequencies also in not completely resolved multiplets have been described in detail in [1] and [2].

A) Preparation and Spectra of the Ethanimines

Cis- and trans-ethanimine were produced by vacuum flash pyrolysis of the trimer, hexahydro-2,4,6-trimethyl-1,3,5-triazine, which, in its hydrated form, was obtained commercially from Aldrich (Steinheim, Germany). Prior to the pyrolysis crystal water and residual impurities were removed by vacuum sublimation and subsequent recristallisation in ethanol. Both isomeric forms, cis and trans, are produced that way, but the thermodynamically less stable cis-isomer [3] is produced predominantly as indicated in the reaction scheme.

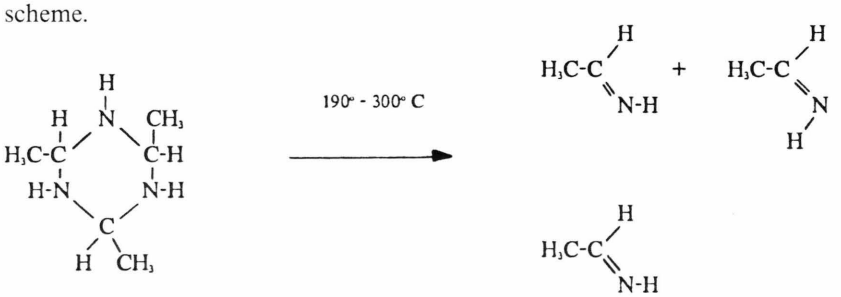

The reason for this may be that the shape of the cis-species is sort of preformed in the trimer with its chair shaped ring and the methyl-groups and amine-hydrogens in aequatorial position. Due to the similarity of their rotational constants, the ratio in which the two isomers were formed could be determined with fairly high precision from the relative intensities in closely neighboured rotational transitions. Accounting for the different dipole moments (the intensities are proportional to the squares of the μ_a or μ_b dipole moment, depending on whether the transition is of μ_a- or μ_b-type [4]) the abundancies were calculated as $n_{cis}:n_{trans} = 12:1$ for a pyrolysis system with an unobstructed rapid flow through the heated zone. This ratio could be changed to approximately $n_{cis}:n_{trans} = 5:1$ if the heated zone was loosely packed with quartz wool. For this comparison the overall flow through the system was maintained at approximately the same level. It was controlled by the pressure drop accross the waveguide absorption cell (20 mTorr at the entrance hole and below 1 mTorr at the exit slit of the cell). Small differences in the Boltzmann factors of the two species were neglected in this calculation of the relative abundancies, and the dipole moments were taken from the work of Lovas et al. [5], i.e. $\mu_a = 2.408\,(14)$ D and $\mu_b = 0.88\,(16)$ D for the trans- and $\mu_a = 0.834\,(23)$ D and $\mu_b = 1.882\,(5)$ D for the cis-species. The absorption cells were cooled to $-50\,^{\circ}C$ in order to increase the population differences between the lower and the upper rotational states and in order to reduce the rate constants for the reactions at the walls.

For the trans-species only μ_a-type spectra could be collected under high resolution conditions because of the less favourable production rate for this species. However for the cis-species the signal to noise ratio was sufficient to allow for the collection of the μ_a-type as well as of the more intense μ_b-type spectra. For both species already the zero field rotational transitions are split into multiplets. The reason for this splitting is twofold.

First hindered internal rotation (torsion) of the methyl group causes a splitting into an A/E-doublet of equal intensity. Both satellites essentially correspond to the vibrational ground state of the methyl torsion. But this state is split into substates due to tunneling. The A-satellite arises from molecules with zero torsional angular momentum, the E-satellite from molecules with a small tunneling angular momentum. For the theoretical background of internal rotation see [6].

Second, ^{14}N quadrupole hyperfine interaction plus spin-rotation interaction cause an additional hfs-splitting of each torsional satellite with hfs-satellites arising from molecules with different orientations of the ^{14}N spin with respect to the rotational angular momentum. Due to the fairly high torsional barriers ($V_3 = 1.475$ kcal/mol for the trans-isomer and $V_3 = 1.595$ kcal/mol for the cis-isomer [5]) the ^{14}N hfs-patterns are experimentally identical for the two torsional states. As an example we present the zero-field multi-

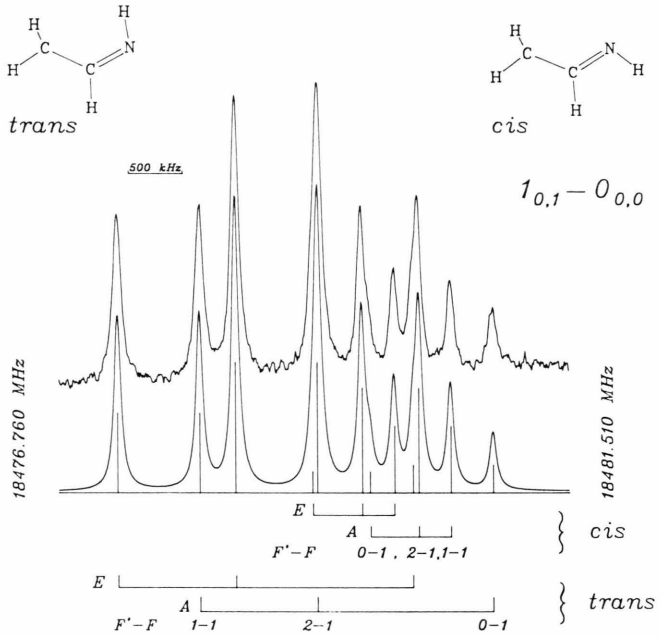

Fig. 1. For cis- and trans-ethanimine the multiplets of the $1_{01} - 0_{00}$ rotational transition fall into the same spectral region. This allows for a comparatively accurate estimate of the relative number densities of the two isomers. The multiplet splitting is caused by methyl internal rotation (A- and E-species) and ^{14}N nuclear quadrupole coupling (see text). For the simulation from the optimized molecular parameters (lower trace) Lorentzian line shapes were assumed. The observed line widths are close to 95 kHz full width at half height.

plets of the $1_{01} \leftarrow 0_{00}$ transition in Fig. 1, which also gives information on the relative abundancies of the cis- and trans-species. For this recording the heated zone was stuffed with quartz wool in order to increase the number density of the trans-species in the pyrolysis products (see above).

The listing of our recorded zero field frequencies, which includes only the frequencies of the hfs satellites of the A-species, is given in Tables 1 (cis-ethanimine) and 2 (trans-ethanimine). In view of the comparatively high barrier, we have analysed the ^{14}N-hfs of both species with the effective rigid rotor Hamiltonian given in Eqs. (2) and (3) of [1]. Our ^{14}N-quadrupole coupling constants and ^{14}N spin-rotation coupling constants, derived from a least squares fit to the splittings of both species are presented in Table 3. For comparison we also present the corresponding results published earlier in [5] and [7]. The accuracy of the quadrupole coupling constants has been improved by two orders of magnitude in the case of the cis-species and by better than one order in the case of the trans-species. They have now reached the quality needed for a critical comparison with new ab initio calculations (see below).

In the case of trans-ethanimine a slight discrepancy between our results and the results presented earlier in [7] is obvious. It is probably due to a misassignment in the earlier publication, where the $4_{04} \leftarrow 3_{13}$ transition of the cis-form was misinterpreted as the $7_{16} \leftarrow 7_{17}$ transition of the trans-form (compare Figure 2). The observed hfs pattern and the simulation from the optimized molecular parameters closely match our assignment (left), while the simulation of the $7_{16} \leftarrow 7_{17}$ pattern not only is predicted at a 13 MHz lower frequency but also shows a significant deviation in the hfs splitting (right). Our assignment is further confirmed by the corresponding hfs-pattern of the torsional E-species measured at 33010.180 MHz ($F' \leftarrow F = 3 \leftarrow 2$), 33010.561 MHz ($F' \leftarrow F = 5 \leftarrow 4$) and 33011.714 MHz ($F' \leftarrow F = 4 \leftarrow 3$), respectively. The differences between the peak frequencies in our observed spectrum (upper left) and the satellite frequencies reported in [7] are due to the fact that our spectrum resulted from upward scans only. The occurrence of such a misinterpretation clearly demonstrates the experimental problems which may arise if different isomeric species are generated by pyrolysis and if their relative abundancies critically depend on the detailed conditions under which the pyrolysis is carried out. We note that in the present investigation the spin-rotation constants of both species could be determined for the first time.

The high field $\Delta M_J = 0$ and $\Delta M_J = \pm 1$ rotational Zeeman effect spectra of both isomers were studied as described in [1]. As an example we present Zeeman multiplets arising from the $1_{01} \leftarrow 0_{00}$ rotational tran-

Table 1. ^{14}N quadrupole hfs splittings of some low-J rotational transitions of cis-ethanimine in the A-torsional state (within our present resolution the hfs of the E-state can not be distinguished from the corresponding A-state patterns). The calculated splittings follow from the optimized coupling constants presented in Table 3. The splittings are given with respect to the hypothetical center frequency: $\Delta v = v - v_0$.

$J'_{K'_-K'_+} \leftarrow J_{K_-K_+}$ v_0/MHz	$F' \leftarrow F$	Relative intensity	$\Delta v_{exp.}$ [MHz]	$\Delta v_{calc.}$ [MHz]	Δ [KHz]
$1_{01} - 0_{00}$	1 – 1	11.10	−0.505	−0.503	−2
18480.138	2 – 1	55.50	−0.050	−0.048	−2
	1 – 0	33.30	0.252	0.248	4
$1_{10} - 1_{01}$	2 – 2	41.70	−0.092	−0.095	3
44469.347	1 – 1	8.33	0.512	0.507	5
	2 – 1	13.90	−0.393	−0.390	−3
	1 – 2	13.90	0.804	0.801	3
	0 – 1	11.10	−1.796	−1.794	−2
	1 – 0	11.10	1.255	1.258	−3
$2_{02} - 1_{01}$	1 – 1	8.33	−0.483	−0.482	−1
36940.263	2 – 1	25.00		−0.022	
			−0.019	−0.018	−1
	3 – 2	46.60		−0.013	
	2 – 2	8.33		0.273	
			0.272	0.271	1
	1 – 0	11.10		0.269	
$2_{12} - 1_{11}$	1 – 0	11.10	−1.251	−1.258	7
35882.199	2 – 2	8.33	−0.981	−0.982	1
	3 – 2	46.60	0.021	0.016	5
	2 – 1	25.00	0.253	0.255	−2
	1 – 1	8.33	1.768	1.771	−3
$2_{11} - 2_{02}$	1 – 2	5.00	−1.253	−1.253	0
45566.913	1 – 1	15.00	−0.792	−0.792	0
	3 – 2	5.19	−0.513	−0.505	−8
	3 – 3	41.50	−0.218	−0.220	2
	2 – 2	23.10	0.782	0.783	−1
	2 – 3	5.19	1.072	1.068	4
	2 – 1	5.00	1.245	1.243	2
$4_{04} - 3_{13}$	3 – 2	23.80	−0.671	−0.671	0
32937.341	5 – 4	40.70	−0.293	−0.293	0
	4 – 3	31.30	0.860	0.861	−1
$4_{23} - 5_{14}$	4 – 5	32.00	−0.988	−0.989	1
31410.531	5 – 6	39.40	0.388	0.390	−2
	3 – 4	25.90	0.643	0.642	1
$5_{23} - 6_{16}$	4 – 5	27.30	−0.644	−0.644	0
33124.471	6 – 7	38.50	−0.385	−0.385	0
	5 – 6	32.40	0.984	0.988	−4

sition of the two isomeric species in Fig. 3, which shows a Zeeman multiplet observed under $\Delta M_J = 0$ selection rule at a field of 15676 Gauss. As in case of the zero-field spectra (compare Fig. 1) the heated zone of the pyrolysis tube was loosely packed with quartz wool for the recording in order to increase the number density of the trans-species downstream of the reaction zone.

In Table 4 we present the molecular g-values and magnetic anisotropies for both isomeric species. The sign of the g-values could be determined unambiguously from intermediate field spectra as described in [8].

Table 2. Zero field ^{14}N quadrupole hfs multiplets observed for trans-ethanimine in the A-torsional state. The calculated splittings follow from the optimized coupling constants given in Table 3. The splittings are given with respect to the hypothetical center frequency: $\Delta v = v - v_0$.

$J'_{K'_-K'_+} \leftarrow J_{K_-K_+}$ v_0/MHz	$F' \leftarrow F$	Relative intensity	$\Delta v_{exp.}$ [MHz]	$\Delta v_{calc.}$ [MHz]	Δ [KHz]
$1_{01} - 0_{00}$	1 – 1	33.30	−0.904	−0.904	0
18478.986	2 – 1	55.50	0.183	0.182	1
	0 – 1	11.10	1.799	1.799	0
$2_{11} - 1_{10}$	1 – 1	8.33	−0.636	−0.636	0
38136.334	2 – 1	25.00	−0.898	−0.899	1
	3 – 2	46.60	0.194	0.195	−1
	2 – 2	8.33	0.000	0.000	−1
	1 – 0	11.10	1.669	1.667	2
$2_{12} - 1_{11}$	2 – 2	8.33	−0.741	−0.743	2
35779.025	2 – 1	25.00	−0.899	−0.899	0
	3 – 2	46.60	0.245	0.244	1
	1 – 0	11.10	1.042	1.044	−2
	1 – 1	8.33	0.627	0.627	0
$2_{02} - 1_{01}$	2 – 2	8.33	−1.094	−1.095	1
36932.272	1 – 0	11.10	−0.894	−0.895	1
	2 – 1	25.00	−0.010	−0.009	−1
	3 – 2	46.60	0.082	0.082	0
	1 – 1	8.33	1.809	1.808	1

Table 3. ^{14}N nuclear quadrupole and spin-rotation coupling constants (in MHz) of cis- and trans-ethanimine resulting from the least squares fit to the hfs-splittings reported in Tables 1 and 2. Uncertainties are one standard deviation from the fit. Also given are the rotational constants which enter into the calculation of the splittings and which are also needed for the subsequent analysis of the data.

cis-ethanimine:		
constant	this work	Lovas et al. [5]
χ_{aa}	0.9980 (22)	0.70 (45)
χ_{bb}	−4.0524 (22)	−3.90 (24)
χ_{cc}	3.0544 (31)	3.20 (37)
M_{aa}	−0.0179 (11)	*.**
M_{bb}	−0.0020 (2)	*.**
M_{cc}	−0.0029 (2)	*.**
B_a = 53120.528 (80) [5]		
B_b = 9778.4950 (106) [5]		
B_c = 8701.3167 (166) [5]		
trans-ethanimine:		
constant	this work	Brown et al. [7]
χ_{aa}	−3.6066 (13)	−3.676 (35)
χ_{bb}	0.5488 (33)	0.552 (16)
χ_{cc}	3.0578 (33)	3.124 (38)
M_{aa}	−0.0114 (11)	*.***
M_{bb}	−0.0062 (7)	*.***
M_{cc}	0.0022 (77)	*.***
B_a = 49960.6 (117) [5]		
B_b = 9828.21 (15) [5]		
B_c = 8650.29 (15) [5]		

B) Preparation, Spectra and Analysis of the Propenimines

The propenimines were prepared by vacuum flash pyrolysis of freshly distilled diallylamine (Aldrich) ac-

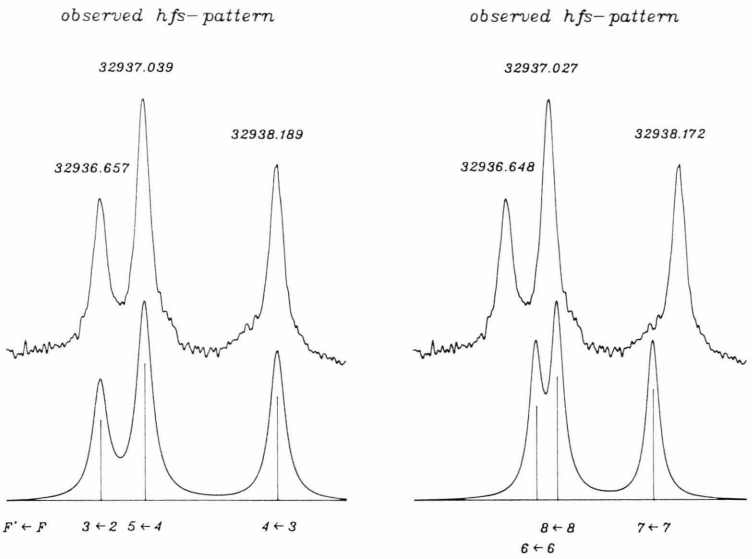

Fig. 2. Observed ^{14}N hfs multiplet of the $4_{04} \leftarrow 3_{13}$ transition of the torsional A-species of cis-ethanimine, which in [7], in the believe that the "cis-spectrum" had too low intensity for detection, has been erroneously assigned to the $7_{16} \leftarrow 7_{17}$ transition of the other isomer, trans-ethanimine.

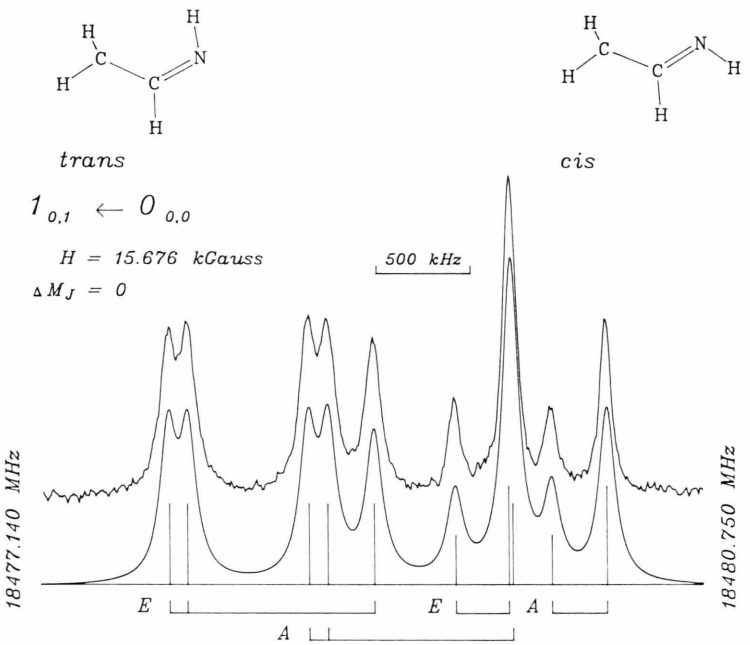

Fig. 3. The $1_{01} \leftarrow 0_{00}$ transition of cis- and trans-ethanimine observed under $\Delta M_J = 0$ and $\Delta M_I = 0$ selection rules (compare Fig. 1 for the zero field multiplet). At the applied field of 15.676 kGauss uncoupling of ^{14}N-spin and overall rotation is essentially complete for the cis-species with its smaller quadrupole coupling constants, while it is still incomplete for the trans-species where the $M_I = 1$ and $M_I = -1$ satellites still show up as separate lines. $M_I = 0$ applies for all satellites. This pattern contains additional information on the magnetic susceptibility.

cording to the following simplified break down scheme:

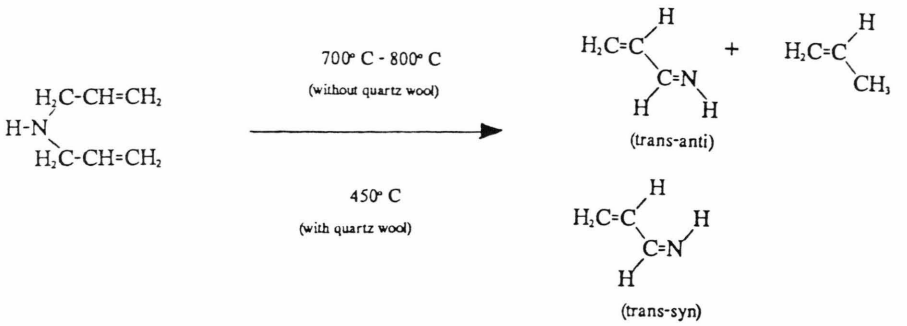

Both isomeric forms trans-anti and trans-syn as well as propene are present downstream from the pyrolysis zone. (No spectroscopic search for other reaction products was carried out in the present study.) Here the thermodynamically more stable trans-anti-species [9] is produced preferentially with a ratio $n_{\text{trans-anti}}/n_{\text{trans-syn}} = 7:1$ calculated from the relative intensities of the $2_{11} \leftarrow 1_{10}$ rotational transition of the two isomeric species. The nomenclature is as follows: "trans" refers to the orientation of the double bonds with respect to the central C–C-bond while "anti" and "syn" refer to the orientation of the N–H-bond with respect to the C–H-bond at the central carbon atom. In the pyrolysis of diallylamine, stuffing of the heated region with SiO_2-wool did not change the trans-anti/trans-syn ratio, but it lowered the optimal temperature range for the pyrolysis to about 450 °C, which indicates a catalytic action.

In accordance with the reported dipole moments $\mu_a = 1.13\,(1)$ D and $\mu_b = 1.66\,(1)$ D for the trans-anti and $\mu_a = 2.39\,(1)$ D and $\mu_b = 0.77\,(2)$ D for the trans-syn [9], μ_a-type as well as μ_b-type transitions could be recorded under high resolution conditions for the more abundant trans-anti-species. For the less abundant trans-syn-species only the μ_a-type spectra had sufficient intensity to allow for high resolution study. In Fig. 4 we show the observed ^{14}N-hfs-pattern of the $1_{01} \leftarrow 0_{00}$ rotational transition for the less abundant trans-syn-species.

Table 4. Molecular g-tensor elements and anisotropies of the molecular magnetic susceptibility (10^{-6} erg G^{-2} mol^{-1}) of cis- and trans-ethanimine resulting from a least squares fit to the observed Zeeman multiplets of the torsional A-species.

		cis-ethanimine	trans-ethanimine
Molecular	g_{aa}	−0.29586 (19)	−0.13144 (10)
Magnetic	g_{bb}	−0.04381 (14)	−0.08347 (9)
g-tensor	g_{cc}	−0.00339 (20)	−0.01221 (9)
		cis-ethanimine	trans-ethanimine
Magnetic Susceptibility Anisotropy	$2\xi_{aa} - \xi_{bb} - \xi_{cc}$	9.32 (32)	0.23 (11)
	$2\xi_{bb} - \xi_{aa} - \xi_{cc}$	8.05 (25)	18.73 (12)

Our zero field frequencies are reported in Tables 5 and 6. The rotational constants [10] and our ^{14}N quadrupole coupling constants and spin-rotation constants, fitted to these observed splittings, are given in Table 7. Also given for comparison are the corresponding values reported earlier by the Monash group [10]. The results will be discussed below with respect to quantum chemical calculations.

From the analysis of the high-field Zeeman splittings the g-values and susceptibility anisotropies listed in Table 8 were obtained. As in the case of the ethanimines, the sign of the g-values could be determined unambiguously from intermediate-field spectra.

Derived Molecular Parameters

As was shown by Flygare and coworkers [11] the theoretical expressions for the elements of the molecular g-tensor and for the magnetic susceptibility tensor may be combined to derive "experimental values" for the molecular electric quadrupole moment tensor and for the anisotropies in the electronic second moments ((14) and (16) in [1], respectively). Since some authors use a definition for the quadrupole moment which differs from ours by a factor of two, we explicitly give our definition:

$$Q_{aa} = (|e|/2)\left[\sum_{n}^{\text{nuclei}} Z_n(2a_n^2 - b_n^2 - c_n^2) - \langle 0|\sum_{j}^{\text{electrons}} (2a_j^2 - b_j^2 - c_j^2)|0\rangle\right] \quad (1)$$

(and cyclic permutations),

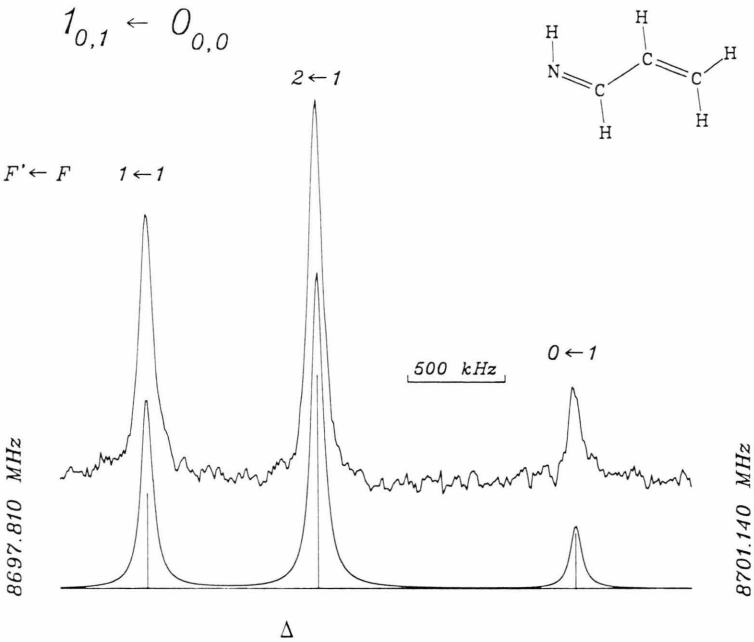

Fig. 4. Zero field ^{14}N hfs pattern for the $1_{01} \leftarrow 0_{00}$ rotational transition of the less abundant trans-syn-species of propenimine. The hfs-pattern scales with $(\chi_{bb}+\chi_{cc})$. The experimental full widths at half height are close to 80 kHz.

Table 5. ^{14}N quadrupole hyperfine splittings of some low-J rotational transitions of trans-anti-propenimine. The calculated splittings follow from the optimized coupling constants presented in Table 7. The splittings are given with respect to the hypothetical center frequency: $\Delta v = v - v_0$.

$J'_{K'_-K'_+} \leftarrow J_{K_-K_+}$ v_0/MHz	$F' \leftarrow F$	Relative intensity	$\Delta v_{exp.}$ [MHz]	$\Delta v_{calc.}$ [MHz]	Δ [KHz]
$1_{10} - 1_{01}$	0 − 1	11.10	−1.751	−1.753	+2
41625.129	1 − 0	11.10	1.140	1.140	0
	2 − 2	41.70	−0.111	−0.111	0
	2 − 1	13.90	−0.336	−0.332	−4
	1 − 1	8.33	0.586	0.583	3
	1 − 2	13.90	0.808	0.804	4
$1_{01} - 0_{00}$	0 − 1	11.10	−0.372	−0.372	0
8709.182	2 − 1	55.50	−0.036	−0.036	0
	1 − 1	33.30	0.183	0.185	−2
$1_{11} - 0_{00}$	1 − 1	33.30	−0.967	−0.967	0
49921.622	2 − 1	55.50	0.198	0.198	0
	0 − 1	11.10	1.912	1.912	0
$2_{11} - 1_{10}$	1 − 1	8.33	−1.742	−1.742	0
17831.059	3 − 2	46.60	−0.121	−0.119	−2
	2 − 1	25.00	0.190	0.189	1
	1 − 0	11.10	0.596	0.595	1
	2 − 2	8.33	1.102	1.105	−3

Table 6. Zero field ^{14}N quadrupole hfs multiplets observed for trans-syn-propenimine. The calculated splittings follow from the optimized coupling constants given in Table 7. The splittings are given with respect to the hypothetical center frequency: $\Delta v = v - v_0$.

$J'_{K'_-K'_+} \leftarrow J_{K_-K_+}$ v_0/MHz	$F' \leftarrow F$	Relative intensity	$\Delta v_{exp.}$ [MHz]	$\Delta v_{calc.}$ [MHz]	Δ [KHz]
$1_{01} - 0_{00}$	1 − 1	33.30	−0.746	−0.751	5
8699.010	2 − 1	55.50	0.150	0.152	−2
	0 − 1	11.10	1.490	1.493	−3
$2_{11} - 1_{10}$	1 − 1	8.33	−0.835	−0.835	0
17828.092	2 − 1	25.00	−0.745	−0.746	1
	3 − 2	46.60	0.146	0.147	−1
	2 − 2	8.33	*.***	0.189	*
	1 − 0	11.10	1.538	1.540	−1
$2_{12} - 1_{11}$	2 − 2	8.33	−0.808	−0.807	−1
16967.939	2 − 1	25.00	−0.749	−0.746	−3
	3 − 2	46.60	0.220	0.218	2
	1 − 0	1.10	0.712	0.709	3
	1 − 1	8.33	0.827	0.826	1
$2_{02} - 1_{01}$	2 − 2	8.33	−0.910	−0.907	−3
17394.457	1 − 0	11.10	−0.746	−0.746	0
	2 − 1	25.00	−0.005	−0.005	0
	3 − 2	46.60	0.068	0.068	0
	1 − 1	8.33	1.498	1.497	1

Table 7. ^{14}N nuclear quadrupole and spin-rotation coupling constants (in MHz) of trans-anti- and trans-syn-propenimine resulting from the least squares fit to the hfs-splittings reported in Tables 5 and 6. Uncertainties are one standard deviation from the fit. Also given are the rotational constants (in MHz) which enter into the calculation of the splittings and which are also needed for the subsequent analysis of the data.

Trans-anti-propenimine:		
constant	this work	Brown et al. [10]
χ_{aa}	0.7414 (11)	0.763 (26)
χ_{bb}	−3.8461 (11)	−3.886 (39)
χ_{cc}	3.1047 (16)	3.123 (55)
M_{aa}	−0.0127 (5)	−0.027 (18)
M_{bb}	−0.0035 (6)	−0.007 (10)
M_{cc}	0.0021 (5)	−0.007 (12)
B_a = 45773.628 (18) [10]		
B_b = 4560.916 (4) [10]		
B_c = 4148.242 (3) [10]		
trans-syn-propenimine:		
constant	this work	Brown et al. [10]
χ_{aa}	−2.9938 (22)	−3.010 (26)
χ_{bb}	−0.1636 (54)	0.041 (68)
χ_{cc}	3.1574 (54)	2.969 (27)
M_{aa}	−0.0103 (18)	*.***
M_{bb}	−0.0022 (11)	*.***
M_{cc}	−0.0022 (11)	*.***
B_a = 43759.52 (18) [10]		
B_b = 4564.581 (39) [10]		
B_c = 4134.423 (30) [10]		

Table 8. Molecular magnetic g-tensor elements and anisotropies of the molecular magnetic susceptibility (10^{-6} erg G^{-2} mol^{-1}) of trans-anti- and trans-syn-propenimine resulting from the least squares fit to the observed Zeeman multiplets.

		trans-anti	trans-syn
Molecular	g_{aa}	−0.46144 (12)	−0.33616 (10)
Magnetic	g_{bb}	−0.04498 (7)	−0.06039 (8)
g-tensor	g_{cc}	−0.00137 (7)	−0.00471 (9)
Magnetic		trans-anti	trans-syn
Susceptibility	$2\xi_{aa}-\xi_{bb}-\xi_{cc}$	18.74 (11)	9.20 (9)
Anisotropy	$2\xi_{bb}-\xi_{aa}-\xi_{cc}$	18.03 (15)	25.95 (12)

$$Q_{ab} = (|e|/2)\left[\sum_{n}^{\text{nuclei}} Z_n 3a_n b_n - \langle 0| \sum_{j}^{\text{electrons}} 3a_j b_j |0\rangle\right]. \tag{2}$$

The diagonal elements Q_{aa} etc. are related to the measured g-values, magnetic susceptibility anisotropies and rotational constants by

$$Q_{aa} = -\frac{h|e|}{16\pi^2 m_p}\left(\frac{2g_{aa}}{B_a} - \frac{g_{bb}}{B_b} - \frac{g_{cc}}{B_c}\right) - \frac{2mc^2}{|e|N}(2\xi_{aa}-\xi_{bb}-\xi_{cc}). \tag{3}$$

Knowledge of the molecular electric quadrupole moments is for instance of interest in the context of understanding the potential hypersurface of van der Waals complexes, which is largely determined by the electric dipole moments, the electric quadrupole moments and the electric polarizabilities of the constituent molecules.

If the structure of the nuclear frame is used as additional input, also "experimental values" for the anisotropies in the electronic second moments may be derived from the Zeeman parameters [12]:

$$\langle a^2-b^2\rangle = \sum_{n}^{\text{nuclei}} Z_n(a_n^2-b_n^2) + \frac{h}{8\pi^2 m_p}\left(\frac{g_{aa}}{B_a} - \frac{g_{bb}}{B_b}\right) + \frac{4mc^2}{3e^2N}\{(2\xi_{aa}-\xi_{bb}-\xi_{cc}) - (2\xi_{bb}-\xi_{cc}-\xi_{aa})\}. \tag{4}$$

(and cyclic permutation).

We present our molecular electric quadrupole moments and anisotropies in the electronic second moments in Table 9. Below we will compare them with the corresponding quantum chemical results.

Theoretical Studies

For comparison with our experimental results we did carry out semiempirical and ab initio quantum chemical calculations. For the semiempirical calculations we did run the INDO-program of Pople and Beveridge [13] with Hamer's extension [14] for the calculation of the molecular electric quadrupole moments. For the ab initio calculation we did run the restricted Hartree-Fock self consistent field (RHF-SCF) routine from the Gaussian 86 program package of Pople and coworkers [15]. The 6-311 G** basis, i.e. triple zeta with polarisation functions (TZVP), p-orbitals at H and d-orbitals at C and N, was used throughout. All quantum chemical calculations were carried out at the "microwave structures" [5, 9].

A) The Molecular Electric Quadrupole Moments and the Anisotropies in the Second Moments of the Electronic Charge Distribution

In Table 9 we present a comparison between our experimental results for the components of the molecular electric quadrupole moment tensor and of the anisotropies in the electronic second moments with the corresponding RHF-SCF-values. A pictorial pre-

Table 9. Experimental values for the molecular electric quadrupole moments in D*Å (see (3)) and the anisotropies in the electronic second moments in Å^2 (see (4)). Also given for comparison are INDO/2 and RHF-SCF-TZVP values calculated at the microwave structures. The last column gives the calculated values for the electronic out-of-plane second moments $\langle c^2 \rangle$. The references for the structures are given below the names of the molecules.

		Q_{aa}	Q_{bb}	Q_{cc}	$\langle a^2-b^2 \rangle$	$\langle b^2-c^2 \rangle$	$\langle c^2 \rangle$
methanimine	exp.	0.44 (17)	1.08 (10)	−1.52 (26)	6.86 (5)	2.14 (6)	
[1]	6-311G**	0.56	1.15	−1.71	6.85	2.10	2.84
	INDO/2	−0.04	1.16	−1.12	6.95	2.17	2.55
trans-	exp.	−5.72 (9)	5.00 (17)	0.72 (17)	23.50 (12)	4.86 (14)	
ethanimine [5]	6-311G**	−5.30	4.97	0.33	23.44	4.81	5.73
	INDO/2	−3.92	4.25	−0.33	23.83	5.50	5.34
cis-	exp.	2.28 (11)	−0.94 (21)	−1.34 (40)	24.85 (15)	4.36 (18)	
ethanimine [5]	6-311G**	1.90	−0.78	−1.12	24.93	4.37	5.77
	INDO/2	3.74	−1.77	−1.97	24.95	4.41	5.34
trans-anti-	exp.	2.20 (11)	1.82 (15)	−4.02 (21)	55.68 (13)	7.73 (10)	
propenimine [9]	6-311G**	2.05	2.12	−4.18	55.54	7.67	5.67
	INDO/2	1.66	1.64	−3.30	55.73	7.85	5.10
trans-syn-	exp.	−4.01 (12)	6.59 (16)	−2.58 (23)	53.91 (13)	8.12 (10)	
propenimine [9]	6-311G**	−4.68	7.15	−2.47	54.08	8.06	5.66
	INDO/2	−5.26	6.91	−1.65	53.04	8.36	5.10

Table 10. Individual components of the molecular magnetic susceptibility tensor as derived from the experimental susceptibility anisotropies (see Tables 4 and 8) and the RHF-SCF-TZVP values for $\langle c^2 \rangle$, which, combined with the experimental g-values and rotational constants, leads to an additional linear equation for the susceptibilities (see (17) in [1]). For error propagation an uncertainty of ±0.1 Å^2 in the $\langle c^2 \rangle$ values was assumed throughout.

	Methanimine	Trans-ethanimine	Cis-ethanimine	Trans-anti-propenimine	Trans-syn-propenimine
χ_{aa}	−8.79 (72)	−26.97 (94)	−23.39 (107)	−23.19 (74)	−26.29 (75)
χ_{bb}	−11.30 (66)	−20.80 (92)	−23.82 (108)	−23.42 (77)	−20.70 (78)
χ_{cc}	−18.96 (72)	−33.37 (109)	−32.30 (134)	−41.69 (86)	−41.07 (87)
χ_{bulk}	−13.02 (70)	−27.05 (100)	−26.50 (116)	−29.43 (79)	−29.35 (80)

sentation of the RHF-SCF-results is presented in Figure 5. For the anisotropies in the electronic second moments the differences between the experimental values and the RHF-SCF values are smaller than 0.2 Å^2, i.e. an agreement within better than two experimental standard deviations. For the molecular quadrupole moments the same statement holds with trans-syn-propenimine the only exception. In view of the fact that no attempt was made to correct the RHF-SCF-values for zero point vibrational effects this agreement appears to us as rather pleasing.

We therefore used the electronic out-off-plane second moments, $\langle c^2 \rangle$, as additional input for a prediction of the bulk susceptibility and of the diagonal elements of the magnetic susceptibility tensor as described for instance in [1]. To our knowledge these values have not yet been determined experimentally before. They are presented in Table 10. For error propagation an uncertainty of ±0.1 Å^2 was assumed in the RHF-SCF-values for $\langle c^2 \rangle$.

B) Spin-Rotation Coupling Constants

Spin-rotation coupling arises from the interaction of the nuclear magnetic dipole moments with the magnetic field caused by the overall rotation of the molecular charge distribution. Since the latter is associated with the rotational angular momentum, while the former are associated with the nuclear spins, the spin-rotation Hamiltonian may be written phaenomenologically as

$$\hat{H}_{SR}/h = -\hat{\mathbf{I}} \cdot \mathbf{M} \cdot \hat{\mathbf{J}}, \tag{5}$$

where the spin-rotation coupling tensor, **M**, depends on the molecular charge distribution. Because of the "$1/r$-dependence", the dominant contribution to **M** arises from the p-electrons localized at the nucleus under consideration while the contributions of the other nuclei and their electronic environment largely cancel. From a detailed theoretical treatment Flygare [16] has derived an approximate expression for the

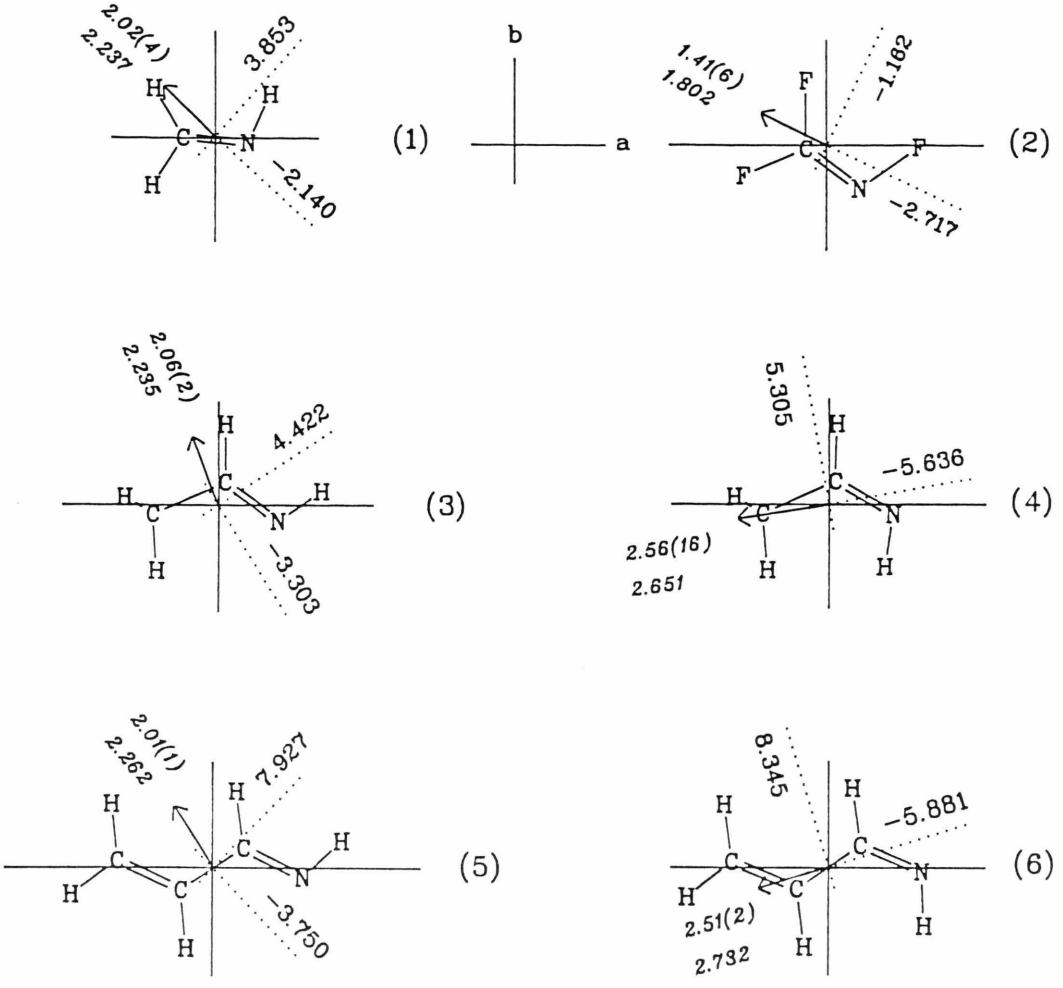

Fig. 5. RHF-SCF (6-311G**) results for the molecular electric quadrupole moment tensors (dotted axes) and the molecular electric dipole moment vectors (SCF- and experimental values in italic) for the five imines studied here. All values are referred to the molecular center of mass. With trifluoromethanimine included for comparison as an exception, the principal axes systems of the molecular quadrupole moment tensors are roughly alligned to the orientation of the lone pair at the nitrogen, with the negative component along this direction. The comparison of the SCF- and experimental results, if referred to the principal inertia axes system (see Table 9), indicates that both are in rough agreement.

M-tensor elements (compare also (5) in [17]):

$$M_{gg} = \frac{-2|e|\mu_n g_N B_g h}{\pi m |\Delta E|} \langle 1/r^3 \rangle_p \cdot [P_{bb} + P_{cc} - P_{bb} P_{cc} + P_{bc} P_{cb}]. \quad (6)$$

In (6) g_N is the ^{14}N nuclear g-value, μ_n the nuclear magneton, $B_g (g = a, b,$ or $c)$ are the rotational constants, h is Planck's constant, $\langle 1/r^3 \rangle = 16.6 \cdot 10^{24}\,\mathrm{cm}^{-3}$ the electronic expectation value for an electron in a nitrogen 2p-orbital [18], c the velocity of light, m the electronic mass, ΔE an average electronic excitation energy, and P_{aa}, P_{bb}, P_{cc}, and $P_{bc} = P_{cb}$ are the density matrix elements at the nitrogen (compare (5) in [1]). We have used INDO p-densities to predict the spin-rotation coupling tensor elements from (6). For the average excitation energies we took the reported $n \rightarrow \pi^*$ excitation energies, since they correspond to the leading terms in the second order perturbation expression which leads to (6).

In Table 11 we list the p-densities and $n \rightarrow \pi^*$ excitation energies. In Table 12 we compare the spin-rotation coupling constants calculated according to (6) to our experimental values. For completeness we have

Table 11. INDO/2 p-density matrix elements at the ^{14}N nuclei (see (5) in [1] and reported $n \rightarrow \pi^*$ excitation energies (references below the values), which were used to predict the ^{14}N spin-rotation coupling constants according to (6). For the rotational constants, which also enter into this equation, see Tables 3 and 7 (the rotational constants of methanimine are given in [1]). The p-densities were calculated at the experimental structures (for the corresponding references see Table 9).

		p_a	p_b	p_c	ΔE/eV
methanimine	p_a	1.2384	−0.1883	0.0000	5.38
	p_b	−0.1883	1.3052	0.0000	[30]
	p_c	0.0000	0.0000	1.0897	
trans-ethanimine		p_a	p_b	p_c	
	p_a	1.4396	0.1107	0.0000	5.43
	p_b	0.1107	1.1007	0.0000	[30]
	p_c	0.0000	0.0000	1.1196	
cis-ethanimine		p_a	p_b	p_c	
	p_a	1.0806	−0.0577	0.0000	5.29
	p_b	−0.0577	1.4557	0.0000	[30]
	p_c	0.0000	0.0000	1.1195	
trans-anti-propenimine		p_a	p_b	p_c	
	p_a	1.1090	0.1107	0.0000	4.46
	p_b	0.1107	1.4324	0.0000	[31]
	p_c	0.0000	0.0000	1.1140	
trans-syn-propenimine		p_a	p_b	p_c	
	p_a	1.4275	0.1830	0.0000	4.46
	p_b	0.1830	1.1540	0.0000	[31]
	p_c	0.0000	0.0000	1.1033	

Table 12. Comparison between the experimental values for the spin-rotation coupling constants with values calculated from the INDO/2 p-densities and $n \rightarrow \pi^*$ energies according to (6). In view of the approximations which lead to (6) the agreement is quite pleasing.

		exp.	calc.
methanimine	M_{aa}	−0.0548 (8)	−0.0556
	M_{bb}	−0.0090 (3)	−0.0099
	M_{cc}	−0.0009 (3)	−0.0082
trans-ethanimine		exp.	calc.
	M_{aa}	−0.0114 (11)	−0.0142
	M_{bb}	−0.0062 (7)	−0.0027
	M_{cc}	0.0022 (7)	−0.0024
cis-ethanimine		exp.	calc.
	M_{aa}	−0.0179 (11)	−0.0145
	M_{bb}	−0.0020 (2)	−0.0028
	M_{cc}	−0.0029 (2)	−0.0024
trans-anti-propenimine		exp.	calc.
	M_{aa}	−0.0127 (5)	−0.0152
	M_{bb}	−0.0035 (6)	−0.0016
	M_{cc}	0.0021 (5)	−0.0011
trans-syn-propenimine		exp.	calc.
	M_{aa}	−0.0103 (18)	−0.0150
	M_{bb}	−0.0022 (11)	−0.0016
	M_{cc}	−0.0022 (11)	−0.0014

also included the $H_2C=NH$ data determined earlier. From this Table it is obvious that Flygares expression (6) predicts the spin-rotation coupling constants with amazing accuracy, a finding which contrasts sharply with earlier statements from the Monash group [19].

C) ^{14}N Nuclear Quadrupole Coupling Constants

The experimental quadrupole coupling constants are related to the vibronic ground state expectation values of the intramolecular electric field gradient tensor, $q_{gg'} = -\left\langle \frac{\partial^2 V}{\partial g\, \partial g'} \right\rangle$, caused by the extranuclear charge distribution as follows:

$$\chi_{gg'} = -|e|\, Q\, q_{gg'}/h \tag{7}$$

(with the indices g and g' running over the molecular axes). Q denotes the nuclear quadrupole moment. e and h the electronic charge and Planck's constant, respectively. For ^{14}N the nuclear quadrupole moment, Q, is on the order of 20 mbarn ($20 \cdot 10^{-27}$ cm^2), but its's accurate value appears to be still disputed. We quote three values from the literature:

$Q(^{14}N) = 17.4\,(2)$ mbarn [20],
$Q(^{14}N) = 19.3\,(8)$ mbarn [21],
$Q(^{14}N) = 20.5$ mbarn [22].

The effective field gradients, q_{aa}, q_{bb}, q_{cc}, etc. arise from two partly compensating contributions, the electronic contribution and the nuclear contribution. Within the rigid nuclear frame approximation they are given as

$$q_{aa} = -\sum_n^{\text{nuclei}} \frac{Z_n |e| \{3a_{nk}^2 - r_{nk}^2\}}{r_{nk}^5} + \langle 0| \sum_j^{\text{electrons}} \frac{|e| \{3a_{jk}^2 - r_{jk}^2\}}{r_{jk}^5} |0\rangle \tag{8}$$

(and cyclic permutations)

for the diagonal elements, and as

$$q_{ab} = -\sum_n^{\text{nuclei}} \frac{Z_n |e|\, 3a_{nk}\, b_{nk}}{r_{nk}^5} + \langle 0| \sum_j^{\text{electrons}} \frac{|e|\, 3a_{jk}\, b_{jk}}{r_{jk}^5} |0\rangle \tag{9}$$

for the off-diagonal element. Here $a_{n,k}$ and $a_{j,k}$ are the a-coordinates of the n-th nucleus and j-th electron with respect to the quadrupole nucleus (and cyclic permutations). While, in the rigid nuclear frame ap-

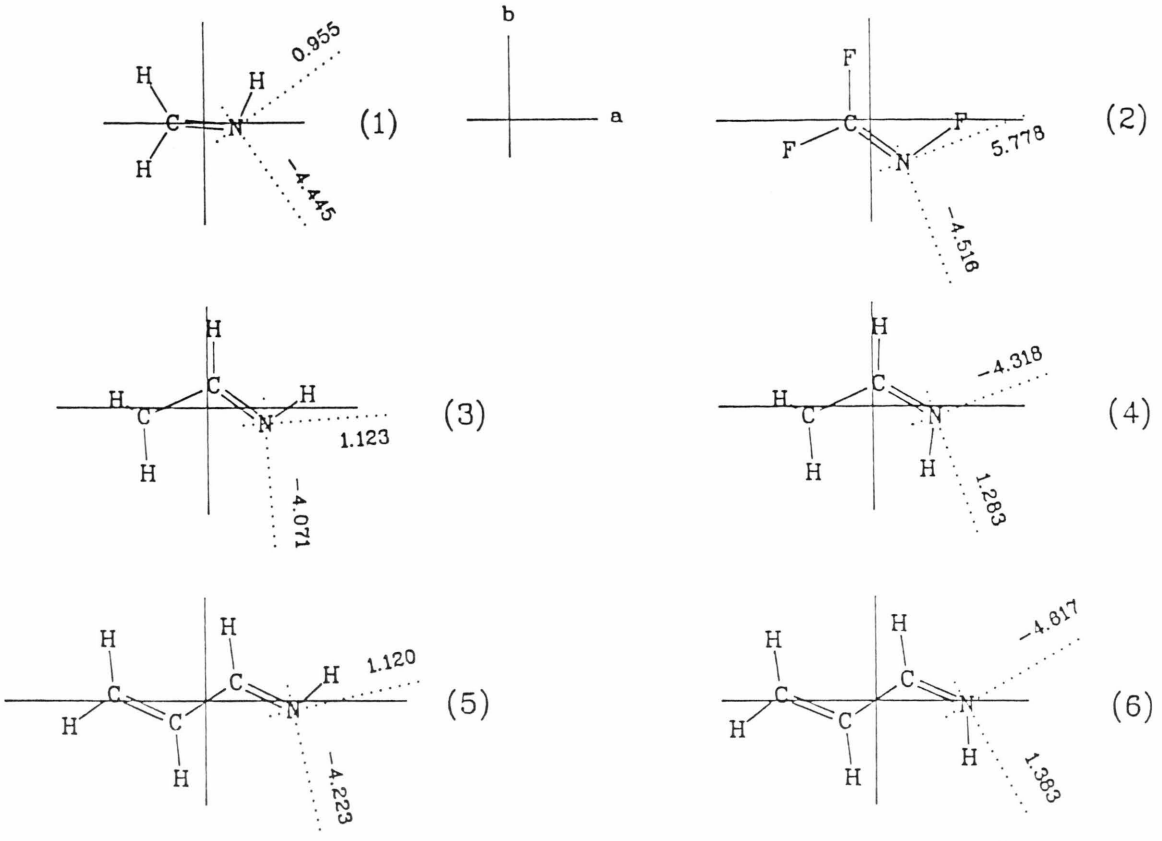

Fig. 6. Pictorial representation of the RHF-SCF (6-311G**) results for the in-plane components of the ^{14}N quadrupole coupling tensors (in MHz). They were calculated at the microwave structures (see text and Table 13). Here a Q-value of 16.84 (15) mbarn was used for the conversion from the field gradients to the coupling constants. This value resulted from a fit for best agreement between the calculated and the experimental data.

proximation, the nuclear contribution is easily calculated from the microwave structure, the accuracy of the electronic contribution depends on the quality of the electronic wavefunction. Thus it's value is method and basis set dependent. Here we have carried out RHF calculations, and a simple way to account for the error in the wavefunction is to multiply the calculated electronic contribution by a basis set dependent calibration factor, f_Q. To our knowledge such a procedure has been proposed first by Brown and coworkers [23], and we too had followed this approach in an earlier publication [24]. However we no more regard this approach as reasonable and prefer to use (7) as it stands with one global Q value as a basis set dependent calibration factor. The reason for this change in mind is as follows. The effect of deficiencies in the electronic wavefunction on the quality of the calculated field gradient depends very much on the region in the molecule where the deficiency occurs. Deficiencies in the neighbourhood of the other nuclei have comparatively little effect, since the main effect of the electronic contribution from these regions is to compensate the contributions from the corresponding nuclei, and this irrespective of minor errors in the electron densities. But deficiencies in the immediate neighbourhood of the quadrupole nucleus have large effects due to the $(1/r^3)$-dependence. Thus, scaling of the electron contribution as a whole as done in [23] and [24] will lead to a correction of the wavefunction errors in the close neighbourhood but also to less compensation of the contributions from the other nuclei. As a result, in a procedure as described above, where two effective Q-values are optimized for best fit between experiment and calculation, the necessity of, say, downscaling the calculated electronic contribution will also lead to an unwanted decompensation of the nuclear contribution and, as a consequence, to the necessity of downscaling also the latter. Therefore in

Table 13. Principal inertia axes values for the nonzero elements of the intramolecular electric field gradient at the imine nitrogen as calculated by the Gaussian 86 RHF-SCF program for the 6-311G** basis, the observed quadrupole coupling constants and the coupling constants calculated from the RHF-SCF field gradients and a basis set dependent conversion factor, which would corresponds to a ^{14}N nuclear quadrupole moment of 16.84 mbarn. This conversion factor results from a least squares fit to the field gradients and coupling constants contained in this Table.

		q/a.u.	χ_{obs}/MHz	χ_{calc}/MHz
methanimine	*aa*	0.213743	−0.9131 (16)	−0.8459
	bb	0.668045	−2.6688 (14)	−2.6438
	cc	−0.881788	3.5819 (21)	3.4896
	ab	−0.643438		
trans-syn-propenimine	*aa*	0.797217	−2.9938 (22)	−3.1550
	bb	0.019879	−0.1636 (54)	−0.0787
	cc	−0.817096	3.1574 (54)	3.2336
	ab	0.797217		
trans-anti-propenimine	*aa*	−0.219202	0.7414 (11)	0.8675
	bb	1.003266	−3.8461 (11)	−3.9704
	cc	−0.784064	3.1047 (16)	3.1029
	ab	−0.286868		
trans-ethan-imine	*aa*	0.928013	−3.6066 (13)	−3.6726
	bb	−0.161010	0.5488 (33)	0.6372
	cc	−0.767004	3.0578 (33)	3.0354
	ab	0.452029		
cis-ethan-imine	*aa*	−0.277728	0.9980 (22)	1.0991
	bb	1.022666	−4.0524 (22)	−4.0472
	cc	−0.744938	3.0544 (31)	2.9481
	ab	−0.090395		
N-methyl-ethanimine [32] (32)	*aa*	−0.347014	1.578 (39)	1.3733
	bb	1.167197	−4.601 (37)	−4.6191
	cc	−0.820183	3.023 (41)	3.2458
	ab	−0.115253		
N-cyanoform-imine [33] (33)	*aa*	−0.572815	2.032 (9)	2.2669
	bb	1.143645	−4.586 (7)	−4.5259
	cc	−0.570830	2.554 (9)	2.2590
	ab	−0.043057		
difluoro-methanimine [35] (36)	*aa*	−0.239158	1.029 (20)	0.9465
	bb	0.632304	−2.560 (17)	−2.5023
	cc	−0.393146	1.531 (22)	1.5559
	ab	−0.441170		
formaldoxime [17] (37)	*aa*	−0.694536	3.0002 (32)	2.7483
	bb	1.194573	−4.6900 (20)	−4.7269
	cc	−0.500037	1.6898 (20)	1.9787
	ab	0.780375		
trifluoro-methanimine [38] (39)	*aa*	−1.130912	4.645 (5)	4.4755
	bb	0.812125	−3.178 (14)	−3.2140
	cc	0.318787	−1.467 (14)	−1.2616
	ab	−0.865017		

$Q = 16.84\,(15)$ mbarn
$\sigma = 0.1423$ MHz

Table 14. Quadrupole coupling constants for two isomeric forms of propargylimine and C-cyanoformimine, respectively, as predicted from RHF-SCF calculations (6-311G**). The conversion factor given in Table 13 was used to calculate the quadrupole coupling constants from the ab initio field gradients. For the propargylimines the discrepancies with respect to the reported experimental values [29] indicate that a reinvestigation under higher resolution should be carried out. For the C-cyanoformimines experimental values are not yet available.

		q/a.u.	χ_{calc}/MHz	χ_{obs}/MHz
E-propargyl-imine	*aa*	−0.231755	0.917	0.1 (3)
	bb	1.138032	−4.503	−3.8 (2)
	cc	−0.906277	3.586	3.7 (4)
	ab	0.115090		
Z-propargyl-imine	*aa*	1.082824	−4.285	−4.1 (2)
	bb	−0.173803	0.688	1.4 (4)
	cc	−0.909021	3.597	2.7 (3)
	ab	0.301513		
E-C-cyano-formimine	*aa*	−0.168823	0.668	
	bb	1.185739	−4.692	
	cc	−1.016916	4.024	
	ab	0.171310		
Z-C-cyano-formimine	*aa*	1.127870	−4.463	
	bb	−0.110368	0.437	
	cc	−1.017502	4.026	
	ab	0.338072		

practice such a two-parameter fit does not improve the fit very much if compared with a one parameter fit in which the calculated field gradient as a whole is scaled with just one gobal effective or pseudo quadrupole moment. On the other hand, the Q-value associated with the nuclear contribution to the field gradient has lost its meaning as the true nuclear quadrupole moment.

Our results are presented in Table 13 and in pictorial form in Figure 6. In addition to the ethanimines and propenimines studied here we also included our results for methanimine [1] and the reported results for difluoromethanimine [25], trifluoro-methanimine [26], N-cyanoformimine [27] and formaldoxime [17]. We note that our $Q(^{14}N)$-value of 16.84 (15) mbarn for the conversion of imine field gradients calculated from RHF-SCF wavefunctions of 6-311 G** quality is also close to Huber's "pseudo quadrupole moment" (17.3 (3) mbarn) proposed to be used with "sp^2-hybridized" ^{14}N nuclei [28].

From the material presented in Table 13 we believe that the ^{14}N quadrupole coupling constants of the "imine-nitrogen" can be predicted within ± 100 kHz from RHF-SCF-wavefunctions of 6-311 G**quality if a microwave structure is available. As examples we take the isomers of propargylimine, H−C≡C−CH=NH, and of C-cyanoformimine, N≡C−CH=NH. For the propargylimines quadrupole coupling constants have been reported in the literature [29]. For C-cyanoformimine, the quadrupole coupling constants are not yet known. We present our SCF-

predictions in Table 14. From the comparison with the reported values we conclude that at least the propargylimine with the acetylene group and the imine-hydrogen in cis position should be reinvestigated since the 1 MHz discrepancy in χ_{cc} is far above our estimate of the uncertainty in the RHF-SCF prediction. To check our predictions, high resolution studies for the cis- and trans-species of both molecules are planned at our laboratory.

Acknowledgements

We are grateful to Prof. Dr. A. Guarnieri for critically reading the manuscript. This work was supported by funds from Deutsche Forschungsgemeinschaft and Fonds der Deutschen Chemischen Industrie. Free computer time at the Rechenzentrum der Universität Kiel is also gratefully acknowledged.

[1] H. Krause, D. H. Sutter, and M. H. Palmer, Z. Naturforsch. **44a,** 1063 (1989).
[2] M. Andolfatto, H. Krause, D. H. Sutter, and M. H. Palmer, Z. Naturforsch. **43a,** 651 (1988).
[3] I. Stolkin, T.-K. Ha, and Hs. H. Günthard, Chem. Phys. **21,** 327 (1977).
[4] C. H. Townes and A. L. Schawlow, Microwave Spectroscopy, McGraw-Hill Book Company, New York 1955, Chapt. 4-2.
[5] F. J. Lovas, R. D. Suenram, D. R. Johnson, F. O. Clark, and E. Tiemann, J. Chem. Phys. **72,** 4964 (1980).
[6] C. C. Lin and J. D. Swalen, Rev. Mod. Phys. **31,** 841 (1959).
[7] R. D. Brown, P. D. Godfrey, and D. A. Winkler, Aust. J. Chem. **33,** 1 (1980).
[8] D. H. Sutter and W. H. Flygare, Topics in Current Chemistry **63,** 143 (1976).
[9] R. E. Penn, J. Mol. Spectrosc. **69,** 373 (1978).
[10] R. D. Brown, P. D. Godfrey, and D. A. Winkler, Chem. Phys. **59,** 243 (1981).
[11] W. Hüttner, M.-K. Lo, and W. H. Flygare, J. Chem. Phys. **48,** 1206 (1968).
[12] W. H. Flygare, Chem. Rev. **74,** 653 (1974).
[13] J. A. Pople and D. L. Beveridge, Approximate Molecular Orbital Theory, McGraw-Hill Book Company, New York 1979.
[14] E. Hamer, L. Engelbrecht, and D. H. Sutter, Z. Naturforsch. **29a,** 924 (1974).
[15] Gaussian 86 User's Guide and Programmer's Reference, M. J. Frisch, J. S. Binkley, H. B. Schlegel, K. Raghavachari, C. F. Melius, R. L. Martin, J. J. P. Stewart, F. W. Bobrowicz, C. M. Rohlfing, L. R. Kahn, D. J. Defrees, R. Seeger, R. A. Whiteside, D. J. Fox, E. M. Fleuder, and J. A. Pople, Carnegie-Mellon Quantum Chemistry Publishing Unit, Pittsburgh PA, 1984.
[16] W. H. Flygare, J. Chem. Phys. **41,** 793 (1964).
[17] A. Klesing and D. H. Sutter, Z. Naturforsch. **45a,** 817 (1990).
[18] R. Barnes and W. H. Smith, Phys. Rev. **93,** 95 (1954).
[19] R. D. Brown, P. D. Godfrey, and D. A. Winkler, Aust. J. Chem. **35,** 667 (1982).
[20] N. Ensslin, W. Bertozzi, S. Kowalski, C. P. Sargent, W. Turchinetz, C. F. Williamson, S. P. Fivozinsky, J. W. Lightbody, and S. Penner, Phys. Rev. C **9,** 1705 (1974).
[21] H. Winter and H. J. Andrä, Phys. Rev. A **21,** 581 (1980).
[22] D. Sundholm, P. Pyykkö, L. Laaksonen, and A. J. Sadlej, Chem. Phys. **101,** 219 (1986).
[23] R. D. Brown and M. P. Head-Gordon, Mol. Phys. **61,** 1183 (1987).
[24] L. Albinus, J. Spieckermann, and D. H. Sutter, J. Mol. Spectrosc. **133,** 128 (1989).
[25] P. Groner, H. Namaie, J. R. Durig, and D. D. DesMarteau, J. Chem. Phys. **89,** 3983 (1988).
[26] D. Christen, J. Mol. Struct. **79,** 221 (1982).
[27] W. H. Stolze and D. H. Sutter, Z. Naturforsch. **44a,** 291 (1989).
[28] S. Gerber and H. Huber, Z. Naturforsch. **42a,** 753 (1987).
[29] M. Sugie, H. Takeo, and C. Matsumura, J. Mol. Spectrosc. **111,** 83 (1985).
[30] R. Ditchfield, J. E. Del Bene, and J. A. Pople, J. Amer. Chem. Soc. **94,** 703 (1972).
[31] V. A. Petukhov, N. E. Agafonov, and I. A. Abronin, Izv. Akad. Nauk, SSSR, Ser. Khim. **2,** 450 (1984).
[32] J. Meier, A. Bauder, and Hs. H. Günthard, J. Chem. Phys. **57,** 1219 (1972).
[33] W. H. Stolze and D. H. Sutter, Z. Naturforsch. **44a,** 291 (1989).
[34] B. Bak and H. Svanholt, Chem. Phys. Lett. **75,** 528 (1980).
[35] P. Groner, H. Namaie, J. R. Durig, and D. D. DesMarteau, J. Chem. Phys. **89,** 3983 (1988).
[36] H. G. Mack, B. Steger, and H. Oberhammer, Chem. Phys. Lett. **129,** 582 (1986).
[37] I. N. Levine, J. Chem. Phys. **38,** 2326 (1963).
[38] D. Christen, J. Mol. Struct. **79,** 221 (1982).
[39] D. Christen, H. Oberhammer, R. M. Hammaker, S. C. Chang, and D. D. DesMarteau, J. Amer. Chem. Soc. **104,** 6186 (1982).